Controlled veiling of silver nanocubes with graphene oxide for improved SERS detection

Martina Banchelli,[a] Bruno Tiribilli,[b] Marella de Angelis,[a] Roberto Pini,[a] Gabriella Caminati,[c]* Paolo Matteini[a]*

[a] Institute of Applied Physics, National Research Council, via Madonna del Piano 10, I-50019 Sesto Fiorentino, Italy

[b] Institute for Complex Systems, National Research Council, via Madonna del Piano 10, I-50019 Sesto Fiorentino, Italy

[c] Department of Chemistry and CSGI, University of Florence, via della Lastruccia 13, I-50019 Sesto Fiorentino, Italy

**p.matteini@ifac.cnr.it, gabriella.caminati@unifi.it*

ABSTRACT

Hybrid graphene oxide (GO)/metal nanocomposites have been recently proposed as novel SERS substrates. Despite an increasing interest in these systems, standardization in their fabrication process is still lacking but urgently required to support their use for real-life applications. In this work we investigate how the assembly of GO should be conducted to control adsorption geometry and optical properties at the interface with plasmonic nanostructures as monolayer assemblies of silver nanocubes, by tuning main experimental parameters including GO concentration and self-assembly time. We finally identified the experimental conditions for building up a close-fitting soft dressing of the plasmonic surface, which shows optimal characteristics for flexible and reliable SERS detection.

keywords: plasmonic nanoparticles; sensing; self-assembly; Raman spectroscopy; quartz crystal microbalance

INTRODUCTION

Surface-enhanced Raman scattering (SERS) spectroscopy is as a robust and versatile analytical technique with the ability to offer detailed and label-free chemical information with molecular selectivity and ultrasensitivity.[1-5] The SERS effect relies on huge electromagnetic fields concentrated at the metal surface of a plasmonic nanostructure, which dramatically enhance the Raman signal of

molecules placed in its close proximity. In this respect, efficient SERS enhancements are typically generated within less than 10 nm from the metal surface and are mostly confined within the so-called "hot spots", i.e. highly curved nanoregions or gaps and junctions between adjacent nanoparticles. The ability to gather molecules in these regions (termed "hot spots") in a homogeneous and reproducible manner represents a current impediment that is still preventing further diffusion of SERS as systematic analytical tool.

A recent trend toward upgrading the performance of SERS technology relies on the combination of plasmonic nanostructures made of silver and gold with graphene.[6-9] Graphene is a single-atom-thick sheet of sp^2-hybridized carbon atoms arranged in a honeycomb lattice. A number of unique chemical, electronic, optical and structural properties make this material a preferred choice for greatly improving electronic and photonic devices.[10-11] With a focus on SERS, current efforts are taking advantage of a thin graphene coating in drawing and concentrating target molecules as well as in conferring the plasmonic surface with a passivating layer that discards possible disturbances and signal variability induced by metal-molecule interactions.[12] Main fabrication methods of graphene sheets include mechanical peel-off, epitaxial growth and chemical vapour deposition (CVD), which, however, appear unsuitable for large-scale production of graphene, ultimately limiting its practical application. A convenient alternative is now represented by graphene oxide (GO), which is derived by oxidation of graphite in the form of graphene sheets with abundant oxygen-containing functionalities. These confer chemical stability in aqueous media or in polar organic solvents owing to electrostatic repulsion between negatively charged sheets and superior versatility in adsorbing different molecular species on its surface as compared to graphene.[13-15] Recent findings also sustained the convenient use of GO and of mild reduced GO in generating SERS signals that accurately resemble the native spectrum of the molecules in solution without frequency shifts, which instead are typically generated as a consequence of the interaction with graphene or metal.[16] Overall, veiling plasmonic nanoparticles with GO sheets is perceived as a favourite strategy to fabricate advanced SERS substrates which hold the promise of improved sensitivity, signal stability and reproducibility.

While complex and laborious procedures are needed for coupling graphene to nanostructured surfaces,[7-8, 17] GO coating can be simply obtained by physisorption of GO sheets in aqueous solution.[18-21] Beside obvious advantages of this approach, a detailed investigation on how the assembly of GO should be conducted to control adsorption geometry and optical properties at the interface is still lacking. In this work we were aimed at verifying the possibility of tuning main experimental parameters (including GO concentration and self-assembly time) in view of engineering effective GO/plasmonic platforms for SERS applications. We finally identified the experimental conditions for

building up a close-fitting soft dressing of the plasmonic surface, which shows optimal characteristics for flexible and reliable SERS detection.

EXPERIMENTAL SECTION

Materials

Ethylene Glycol (EG, ≥ 99%) was obtained from Scharlab. Sodium sulphide nonahydrate, PVP (M_w 55000), silver nitrate, GO solution (4 mg mL^{-1}) and R6G were obtained by Sigma Aldrich. Aqueous solutions were prepared using ultrapure Milli-Q water. Silicon wafers (N-type, no dopant) were purchased from Sigma Aldrich.

Synthesis of AgNCs

EG (10 mL) was placed into a flask and heated under magnetic stirring in an oil bath at 150 °C for 1 h under a nitrogen flow. Then, 0.175 mL of a 0.72 mg mL^{-1} sodium sulphide solution and 3.75 mL of a 20 mg mL^{-1} PVP solution in EG were subsequently added to the flask. The flask was thermostated for additional 10 min, until a temperature of 150 °C was again established. A silver nitrate solution (1.25 mL) in EG with a concentration of 48 mg mL^{-1} was added dropwise to the reaction flask at a rate of approximately 1 mL min^{-1}. The reaction was stopped after 40 min by placing the flask in an ice-bath and by adding 30 ml of acetone. Nanoparticles were then centrifuged at 10000 g for 30 min and then dispersed in ethanol or chloroform by using an ultrasonic bath. The washing procedure was repeated at least three times in order to ensure the complete removal of the reagents. The suspensions of AgNCs thus obtained were stored in centrifuge tubes at -20 °C.

Langmuir-Blodgett AgNCs film preparation

A KSV3000 trough (KSV Instruments Ltd., Finland) filled with Milli-Q water (resistivity =18 MΩ cm, pH = 5.6 at 20 °C) was used to prepare the Langmuir monolayers under symmetric compression. 1.65 mL of a 3.1 mg mL^{-1} suspension of AgNCs in chloroform was dropwise deposited over the water surface and the monolayer was kept undisturbed for additional 40 min to allow complete chloroform evaporation. Compression of the monolayer was achieved by moving inwards the barriers with a compression speed of 20 mm min^{-1}. The surface pressure of the subphase was measured with a platinum Wilhelmy plate as a function of the surface area per nanocube (taken = 50 nm). Langmuir-Blodgett films were transferred onto cleaned quartz and silicon substrates by vertical dipping at a rate of 2 mm min^{-1}, at different surface pressures. Monolayers of AgNCs were transferred on SiO_2-covered QCM quartz sensors through the same procedure. All substrates were cleaned with ethanol and dried under nitrogen. The reported results are the average of at least three independent measurements.

Quartz Crystal Microbalance measurements

QCM experiments with impedance monitoring were performed on a QCM-Z500 (KSV Instruments Ltd) equipped with a thermoelectric (TE) module (Oven Instruments). The resonant frequency shift and the change in energy dissipation of a SiO_2-coated AT-cut 5 MHz quartz microcrystal were simultaneously measured at its resonant frequency and at the third, fifth, seventh, ninth and eleventh overtones. The temperature of the measuring cell was kept constant at 20 °C with a Peltier element connected to the TE module. Frequency and admittance data were simultaneously recorded and taken into consideration for the analysis. The QCM experimental data were analysed by means of the commercial QCMBrowse analysis software to estimate adsorbed mass and film thickness. [22]

AFM measurements

Non-contact AC mode atomic force microscopy (AFM) images were acquired in air using a PicoSPM microscope equipped with an AC-mode controller (Keysight Technologies, Inc formerly Molecular Imaging). For optimal resolution rectangular non-contact gold-coated cantilever were used (model Hi'Res-C14 from MicroMash - www.spmtips.com), with typical resonance frequency of 160 kHz, and 1 nm tip radius. Nanocubes sizes were measured from the height statistics in the topographic AFM images. Image processing and pseudo 3D rendering has been performed using Gwyddion 2.30 SPM data visualization tool (http://gwyddion.net/).

SERS measurements

Raman measurements were performed at room temperature on an XPlora Horiba MicroRaman with a 638 nm laser as excitation source. We used a 100× objective with accumulation times of 10 s per spectrum and a 70-μW power on the sample. A 2 10^{-4} M R6G solution in water was prepared by diluting a stock ethanolic 10^{-2} M solution. The SERS substrates were pre-immersed in this solution for two hours to ensure that adsorption equilibrium was reached, then rinsed with deionized water and dried under nitrogen flux before each SERS measurement. The accumulation times and the laser power were the same for all Raman measurements. R6G was selected as model target compound on consideration of its potential to establish π-π, electrostatic and H-bond interactions as well as to its general use as SERS probe for both metallic and graphene substrates. Methods used for FEM modelling and EF calculation are described in Supporting Information.

RESULTS AND DISCUSSION

We started with fabricating monolayer assemblies of silver nanocubes (AgNCs) as a convenient nanostructured basal layer for the following deposition of GO. From one side, the availability of a solid synthesis protocol ensures accessibility to colloidal batches of AgNCs with high monodispersity

and formation yield.[23] Additionally, AgNCs represent a popular choice in SERS owing to intense electromagnetic fields localized at their corners, which are further intensified in the gap regions between closely spaced nanoparticles [24]. The as-synthesized AgNCs (Figures S1-S3) were assembled in monolayers by means of the Langmuir-Blodgett (LB) technique.[25-26] By using an optimal surface pressure of 15 mN m^{-1} (Figure S4) a secure transfer of the nanoparticle assemblies to quartz and silicon substrates was obtained. Typical assembly patterns include regions of tightly packed nanoparticles with average interparticle gaps of 1-2 nm and recurrent face-to-face orientation as well as a 5% of isolated nanoparticles (Figure 1). This picture is responsible for a multi-peak centred at 410 nm and another broad peak at 650 nm corresponding to the plasmon resonances of isolated and assembled AgNCs, respectively (Figure S5).[27]

One-atom-thick GO sheets with lateral dimensions of few microns (Figure S6) were then deposited on the AgNCs layer. The adsorption process was followed by a quartz crystal microbalance (QCM) with dissipation monitoring.[28] The technique outputs main parameters such as frequency shift, which is proportional to the adsorbed mass accumulated onto the sensor surface, and energy dissipation, which reflects the structural/viscoelastic properties of the adsorbed layer. In brief, an AgNCs LB monolayer on a quartz substrate was exposed to a GO dispersion, which was added to the QCM chamber at increasing concentration. Precisely, the AgNCs surface was sequentially exposed to more concentrated GO as long as frequency and dissipation reached a saturation level.

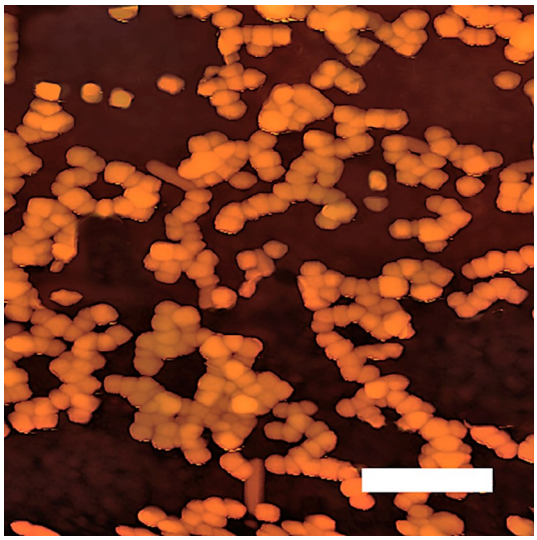

Figure 1. AFM topography of an AgNCs LB monolayer (Bar = 500 nm)

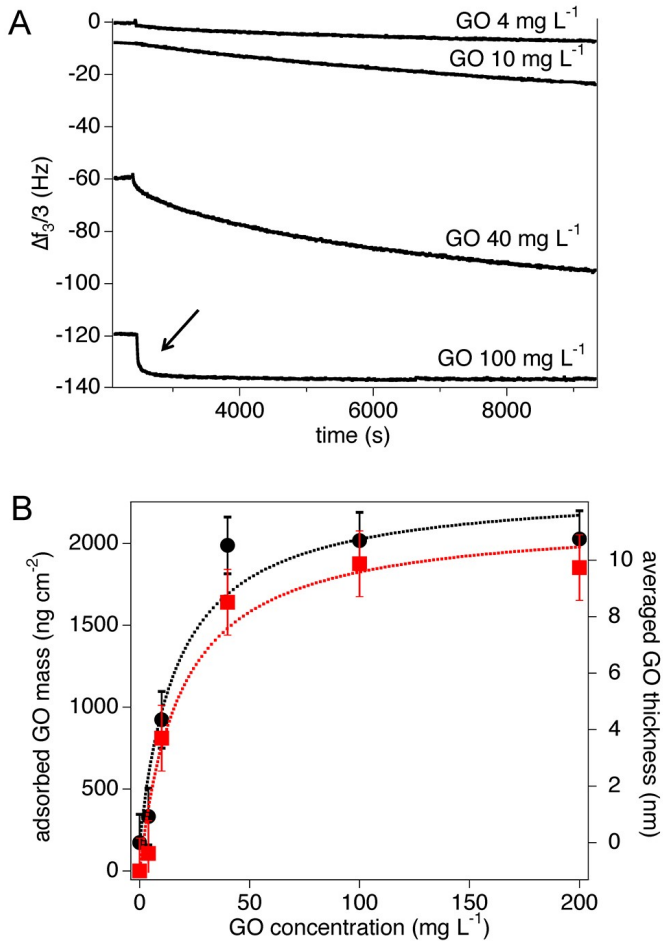

Figure 2. a) QCM frequency shifts (relative to the third overtone of the quartz frequency) recorded during exposure of an AgNCs monolayer to GO solutions at different concentration. Arrow indicates the time needed to reach the equilibrium condition at 100 mg L^{-1}, i.e. ≈40 min. b) Adsorbed mass (squares) and thickness (circles) as computed by a two-layer model.[22] The surface area of quartz sensor available for GO deposition was 78.5 mm^2, including a 70% of space occupied by AgNCs.

Our findings clearly evidenced that at 100 mg L^{-1} GO, the (negative) frequency shift is the largest and remains unchanged upon further addition of GO (Figure 2a). We anticipate that the equilibrium condition corresponds to the maximum GO adsorption capacity on the AgNCs layer and further GO adsorption is prevented by repulsive interactions with the as-formed GO layer. Additionally, the changes in dissipation values at different concentration of adsorbed GO (Figure S7) can be correlated to the viscoelastic properties of the deposited GO layer. As the density of adsorbed GO increases, dissipation significantly increases, which suggests that the GO sheets are not adsorbed flat onto the AgNCs surface and that the adsorbed layer is not rigidly structured but assembled as a soft matter.

Adsorbed mass and layer thickness of GO on the AgNCs monolayer were then estimated by means of a fitting model,[22] which takes into account for both a rigid and a viscoelastic layer adsorbed onto the

sensor surface.[28] The adsorbed GO mass at saturation was found to be 108, 810, 1640 and 1850 ng cm^{-2} for 4, 10, 40 and 100 mg L^{-1} of GO added, respectively. A certain degree of nonideality is predicted due to two main factors: firstly, wrinkling and folding of GO sheets on the metal surface can occur[29] while stacking of multiple layers appears less plausible according to the flexibility ascribed to micrometric GO as revealed by QCM results and supported by previous reports;[30-31] secondly, water molecules can be retained by GO sheets both at the rim of them and as trapped at the AgNCs/GO interface.[32-33] The latter may contribute to up to about 30% in weight of the mass detected, which thus includes both the actual GO mass and the water associated to it.[34] According to a Langmuir-type mechanism (Figure 2b, red curve), and considering $CK_d^{-1} = \Theta/(1-\Theta)$, where C is the GO concentration and $\Theta = (\Delta m/A)/(\Delta m/A)_{sat}$ is the surface coverage, a pseudo-dissociation constant K_d of 18.2 mg L^{-1} is retrieved.

The calculated average thickness increases from a minimum of 1 nm to a maximum of 11 nm as a function of GO bulk concentration (Figure 2b, black curve). Similarly to above, an increase in thickness can be correlated to hydration effects and sheet wrinkling on the AgNCs surface. The latter prevails for dense assemblies of GO and may reasonably lead to coatings thicker than 1 nm, that is the thickness of a flat single GO sheet (Figure S6).[31, 35]

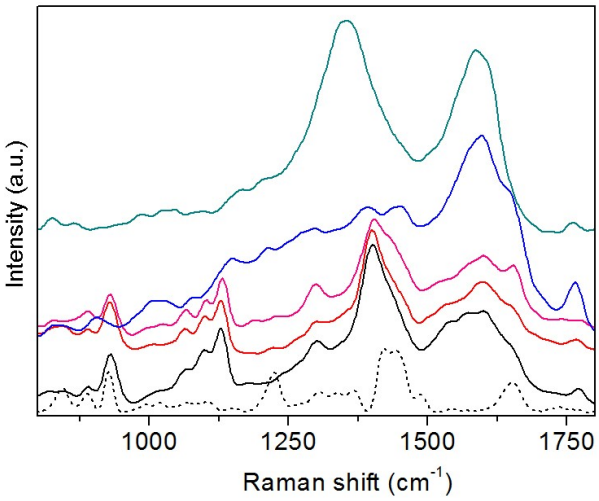

Figure 3. Raman spectra of AgNCs@GO assemblies fabricated by using 0, 4, 10, 40, 100 mg L^{-1} GO dispersions (solid line, from bottom to top) and of PVP (dotted line).

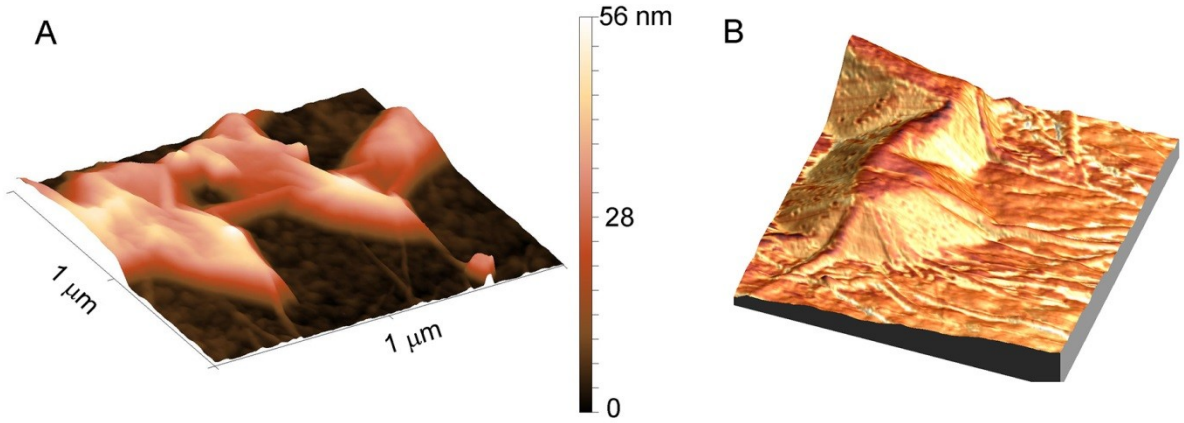

Figure 4. AgNCs@GO assembly at 100 mg L^{-1} GO: 3D AFM topography (a) and 3D topography with the phase map used as texture (b).

Further insights into the self-assembly process were obtained by analysing the different Raman profiles of the fabricated AgNCs@GO assemblies (Figure 3). The G band at around 1601 cm^{-1} and the D band at around 1365 cm^{-1}, which represent the tangential stretching mode of the E_{2g} phonon of sp^2 atoms and the breathing mode of κ-point phonons,[36] are characteristic spectral features of GO. These two bands appeared 500-fold enhanced in the 100 mg L^{-1} AgNCs@GO sample as a result of the electromagnetic enhancement generated by the underlying silver layer (Figure S8). For lower concentration values, i.e. 4 and 10 mg L^{-1}, the GO bands are masked by contributions assigned to impurities derived from the nanoparticle synthesis, mostly the capping agent PVP (Figure 3). The GO profile starts to prevail at 40 mg L^{-1}. However, a dramatic point to point signal variability was observed in this case, while the signal becomes stable at 100 mg L^{-1} GO. This behaviour is in line with an initial adhesion of isolated GO sheets loosely interacting with the underlying metal layer followed by formation of tight GO/metal interactions once an equilibrium state is reached. From a chemical perspective, the driving step of the self-assembly can be mainly assigned to the formation of hydrophobic interactions between the hydrocarbon backbone of PVP and the sp^2 domains of GO. Once few GO sheets are anchored to the Ag surface, the remaining assembly process should be regulated by the competition between electrostatic repulsion and van der Waals attraction forces between GO sheets as previously theorized for a GO monolayer at a water interface.[31, 37] At low GO sheets density the former forces prevail because of negative charges at the sheet edges originating from ionized carboxylic acid groups. However when the sheets come closer as a consequence of crowding, face-to-

face van der Waals interactions arise eventually inducing a close-packed layer containing folded and wrinkled patterns.[29, 37-38]

The AFM analysis confirmed the above suppositions revealing a soft and homogeneous veil-like membrane overlapping the AgNCs with ridges of GO departing from the cube corners (Figure 4). The adsorbed GO has an average thickness of 7 nm (Figure S9), which supports the formation of wrinkled geometries within single and between adjoining sheets after their adhesion to the nanoparticle surface, as discussed above.

Summarizing, a stable GO assembly over an AgNCs layer is obtained at a saturation level of GO sheets, but at the expense of a substantial increase in thickness of the GO layer. Remarkably, previous investigations suggested the requirement of using very thin, i.e. single-atom-thick, graphene coatings when sensitive SERS applications are concerned.[8] In fact the thicker the graphene layer, the larger the distance between adsorbed molecule and EM enhancing surface beneath, the lower should become the SERS signal detected.

The nanoscale distribution of the E-field enhancement as simulated by a finite element method (FEM) confirmed the latter prevision (Figure 5). The theoretical calculations evidenced that the maximum $-\!\!\blacktriangleleft E/E0\triangle^2$ intensity is 70% reduced when a 7 nm-thick GO layer is added on the surface of AgNCs (compare Figure 5a and Figure 5 c). Interestingly, the corresponding E-field distribution in the absence of GO and observed at a 7 nm distance from the Ag surface appears more confined (compare Figure 5c and Figure 5d). Thus GO appears to play an active role in the distribution of the local electric field that can be probably ascribed to its recognized polarizability properties mainly originating from its high oxygen content (which also makes it a superior substrate with respect, e.g., to graphene).[39] This effect is further apparent when a cluster of cubes is considered. In particular a more spread E-field distribution along the cluster edges and at the interface between particles is generated after supporting a 7 nm-thick GO layer on four packed cubes, which contrasts with well-localized hot spots observed for bare cubes (compare Figure 5e and 5f).

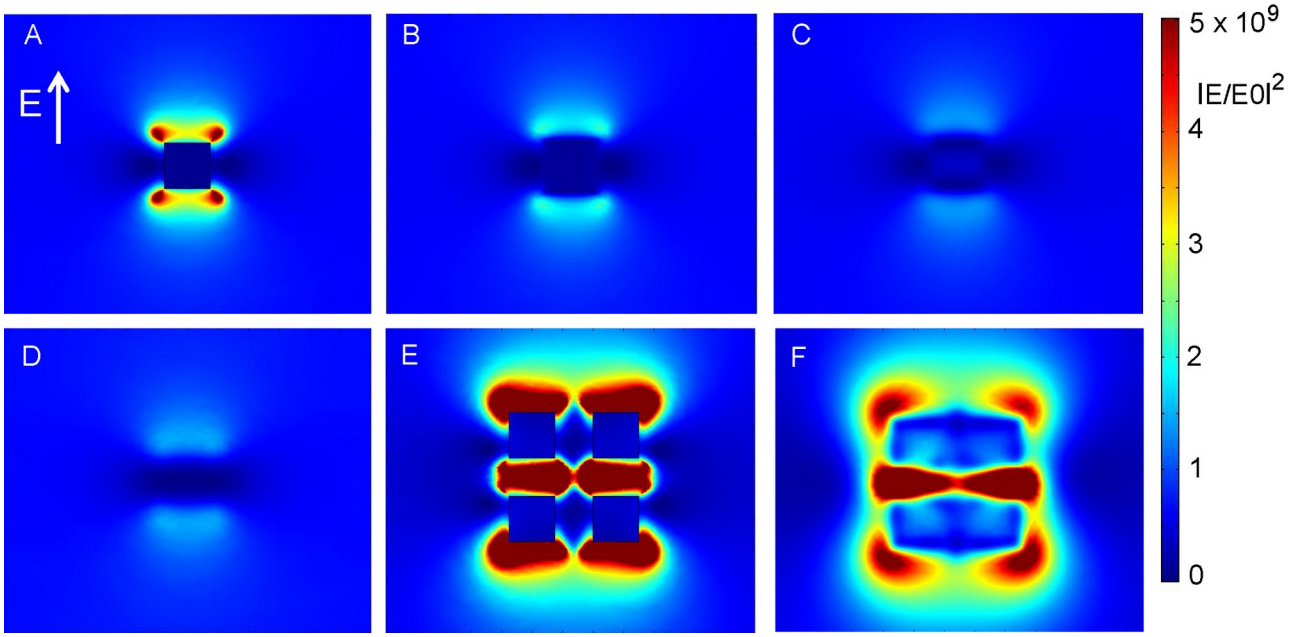

Figure 5. FEM simulation of the spatial distribution of the E-field for isolated cubes (a-d) and for 4-cube clusters (e,f) without (a,e) and with a 1-nm thick (b) or a 7 nm-thick (c,f) graphene layer. The $|E/E0|^2$ value is calculated on top of the cube (a,e) or of the GO layer (b,c,f) or at a 7 nm distance from the cube in the absence of a GO layer (d).

With this in mind, we carried out SERS measurements to experimentally investigate the consequences of GO veiling over the signal behaviour. The results pointed out a superior SERS activity of the substrate containing a GO coating, including more resolved peaks with higher signal intensity and larger reproducibility. For example, in the SERS spectrum of R6G even weaker Raman peaks (e.g. see the region around 600 cm^{-1}) can be identified (Figure 6). Moreover, we found three-fold stronger enhancement factor (EF) values for the GO-veiled with respect to the bare AgNCs substrates (Figure 6, Figure S10). These results conflict with the FEM simulation indicating a substantial decrease in the E-field intensity after addition of a GO layer while suggest the occurrence of a positive net effect secondary to the introduction of GO. First, the latter can account for an additional chemical enhancement conferred by a combination of π-π interactions and charge transfer from the oxygen-rich functional groups of GO to the probe molecules.[16] Additionally, GO is considered a molecular catcher toward different compounds that therefore are accumulated on its surface, in turn intensifying the SERS signal.[12]-

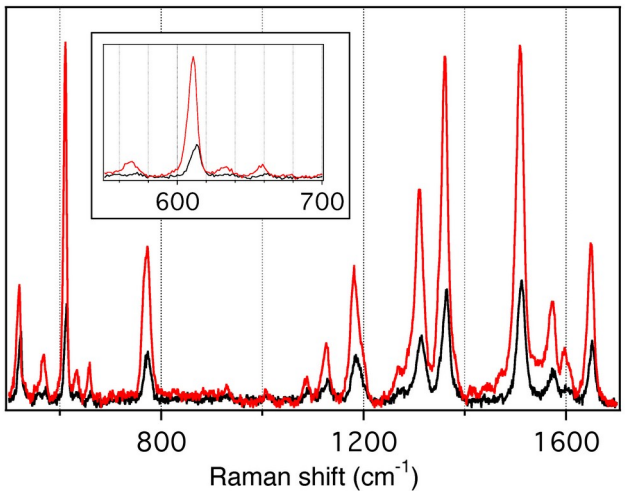

Figure 6. SERS spectrum of R6G adsorbed on bare AgNCs (black) and on a AgNCs@GO assembly (red). Inset: enlargement of the region centred at 610 cm^{-1}.

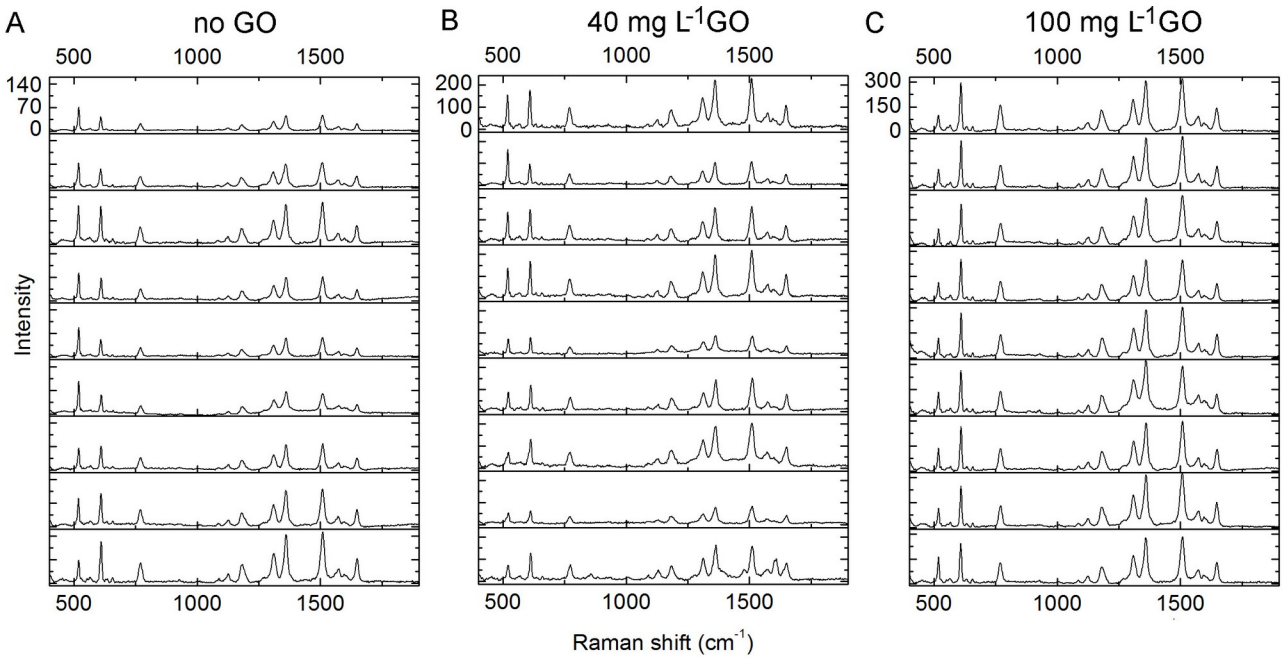

Figure 7. Random spectra of R6G obtained by point-to-point mapping over 50×50 μm^2 areas from AgNCs substrates coated by using 0 mg L^{-1} (a), 40 mg L^{-1} (b) and 100 mg L^{-1} (c) GO (4 replicates per concentration). The standard deviation values of the intensity referred to the 1510 cm^{-1} peak are: 39% at 0 mg L^{-1}, 43% at 40 mg L^{-1} and 17 % at 100 mg L^{-1} GO.

Most importantly, a distinctively uniform SERS signal was detected by point-to-point mapping over large areas (50×50 μm^2) of substrates veiled with 100 mg L^{-1} GO (Figure 7c). The reproducibility is dramatically reduced in the absence of GO or in the case of an uncompleted or loose GO covering as occurs for the 40 mg L^{-1} sample (Figures 7a,b). In conclusion we deduce that providing plasmonic

substrates with a close-packed GO coating becomes a valuable solution to obtain bright and intense signals and to overcome signal fluctuations usually caused by variable molecular interactions with the metal. These results confirm previous observations on the convenience of supplying plasmonic substrates with a thin passivating graphene layer and also shed light on the possibility to improve SERS detection on adjusting experimental parameters that regulate the physisorption of GO sheets. Substrates partially or weakly covered by GO as those obtained at low concentration and self-assembly time of GO sheets have been shown to suffer from scarce reproducibility and low SERS signals. Conversely a chance for generating stable and intense SERS responses is provided by maximizing the GO adsorption capacity on the plasmonic substrate.

CONCLUSION

In this paper we stress how structuring and thickness of a GO covering layer may influence SERS molecule detection. Plasmonic substrates with a close-fitting GO dressing exhibit improved SERS performances, including intense and reproducible signals. Remarkably, we showed that by a safe and simple GO deposition process based on GO self-assembly on metal surface an effective coating can be obtained at saturation levels of GO sheets. Concurrently, an overall thickening of GO layer is induced, which, however, appears favourable in generating uniform and intense SERS signals, despite the molecule is distanced from the plasmonic surface. These results appear thus propaedeutic in the design and fabrication of optimized GO-veiled platforms with reliable and effective SERS activity for molecular detection and sensing. Notably, the twofold nature of GO bringing both polar and apolar moieties and its unique capability to impart the plasmonic metal substrate with a soft dressing offer potential for future development of flexible SERS assays of different targets of interest in analytical, medical, biomedical and pharmaceutical application fields.

ASSOCIATED CONTENT

Supporting Information

Description of the AgNCs synthesis; UV-vis spectra of AgNCs at different reaction times; TEM of AgNCs; distribution of the variability of the synthesized AgNCs; description of the Langmuir-Blodgett assembly process; UV-vis absorbance spectra of AgNCs and AgNCs@GO assemblies; AFM of GO sheets; dissipation monitoring of GO assembly by QCM; comparison between the SERS profiles of GO sheets and of AgNCs@GO assemblies; description of the procedure for calculating the Enhancement Factor; description of the procedure for FEM modelling

ACKNOWLEDGEMENTS

This work was partially supported by Tuscany Region and European Community within the frame of the ERANET+ Project BI-TRE, by the Tuscany Region SUPREMAL project and by MIUR (Italian Ministry of Education, Universities and Research).

REFERENCES

(1) Willets, K. A.; Van Duyne, R. P. Localized Surface Plasmon Resonance Spectroscopy and Sensing. *Annu. Rev. Phys. Chem.* **2007,** *58*, 267-297.
(2) Moskovits, M. Surface-Enhanced Spectroscopy. *Rev. Mod. Phys.* **1985,** *57*, 783-826.
(3) Alvarez-Puebla, R. A.; Liz-Marzan, L. M. Traps and Cages for Universal Sers Detection. *Chem. Soc. Rev.* **2012,** *41* (1), 43-51.
(4) Kneipp, J.; Kneipp, H.; Kneipp, K. Sers - a Single-Molecule and Nanoscale Tool for Bioanalytics. *Chemical Society Reviews* **2008,** *37* (5), 1052-1060.
(5) Pahlow, S.; Marz, A.; Seise, B.; Hartmann, K.; Freitag, I.; Kammer, E.; Bohme, R.; Deckert, V.; Weber, K.; Cialla, D.; Popp, J. Bioanalytical Application of Surface- and Tip-Enhanced Raman Spectroscopy. *Eng. Life Sci.* **2012,** *12* (2), 131-143.
(6) Lee, J. U.; Lee, W.; Yoon, S. S.; Kim, J.; Byun, J. H. Site-Selective Immobilization of Gold Nanoparticles on Graphene Sheets and Its Electrochemical Properties. *Appl. Surf. Sci.* **2014,** *315*, 73-80.
(7) Li, X.; Choy, W. C. H.; Ren, X.; Zhang, D.; Lu, H. Highly Intensified Surface Enhanced Raman Scattering by Using Monolayer Graphene as the Nanospacer of Metal-Film-Metal Nanoparticle Coupling System. *Adv. Funct. Mater.* **2014,** *24*, 3114-3122.
(8) Xu, W.; Xiao, J.; Chen, Y.; Chen, Y.; Ling, X.; Zhang, J. Graphene-Veiled Gold Substrates for Surface-Enhanced Raman Spectroscopy. *Adv. Mater.* **2013,** *25*, 928-933.
(9) Zhao, Y.; Li, X.; Du, Y.; Chen, G.; Qu, Y.; Jiang, J.; Zhu, Y. Strong Light-Matter Interactions in Sub-Nanometer Gaps Defined by Monolayer Graphene: Toward Highly Sensitive Sers Substrates. *Nanoscale* **2014,** *6*, 11112-11120.
(10) Shao, Y. Y.; Wang, J.; Wu, H.; Liu, J.; Aksay, I. A.; Lin, Y. H. Graphene Based Electrochemical Sensors and Biosensors: A Review. *Electroanalysis* **2010,** *22* (10), 1027-1036.
(11) Wang, X.; Zhi, L. J.; Mullen, K. Transparent, Conductive Graphene Electrodes for Dye-Sensitized Solar Cells. *Nano Lett.* **2008,** *8* (1), 323-327.
(12) Xu, W.; Mao, N.; Zhang, J. Graphene: A Platform for Surface-Enhanced Raman Spectroscopy. *Small* **2013,** *9*, 1206-1225.
(13) Liu, J. B.; Fu, S. H.; Yuan, B.; Li, Y. L.; Deng, Z. X. Toward a Universal "Adhesive Nanosheet" for the Assembly of Multiple Nanoparticles Based on a

Protein-Induced Reduction/Decoration of Graphene Oxide. *J. Am. Chem. Soc.* **2010,** *132* (21), 7279-7281.
(14) Dreyer, D. R.; Park, S.; Bielawski, C. W.; Ruoff, R. S. The Chemistry of Graphene Oxide. *Chem. Soc. Rev.* **2010,** *39* (1), 228-240.
(15) Geng, J. X.; Jung, H. Porphyrin Functionalized Graphene Sheets in Aqueous Suspensions: From the Preparation of Graphene Sheets to Highly Conductive Graphene Films. *J. Phys. Chem. C* **2010,** *114* (18), 8227-8234.
(16) Yu, X. X.; Cai, H. B.; Zhang, W. H.; Li, X. J.; Pan, N.; Luo, Y.; Wang, X. P.; Hou, J. G. Tuning Chemical Enhancement of Sers by Controlling the Chemical Reduction of Graphene Oxide Nanosheets. *ACS Nano* **2011,** *5* (2), 952-958.
(17) He, S. J.; Liu, K. K.; Su, S.; Yan, J.; Mao, X. H.; Wang, D. F.; He, Y.; Li, L. J.; Song, S. P.; Fan, C. H. Graphene-Based High-Efficiency Surface-Enhanced Raman Scattering-Active Platform for Sensitive and Multiplex DNA Detection. *Anal. Chem.* **2012,** *84* (10), 4622-4627.
(18) Huang, J.; Zhang, L. M.; Chen, B. A.; Ji, N.; Chen, F. H.; Zhang, Y.; Zhang, Z. J. Nanocomposites of Size-Controlled Gold Nanoparticles and Graphene Oxide: Formation and Applications in Sers and Catalysis. *Nanoscale* **2010,** *2* (12), 2733-2738.
(19) Li, Y. G.; Wu, Y. Y. Coassembly of Graphene Oxide and Nanowires for Large-Area Nanowire Alignment. *J. Am. Chem. Soc.* **2009,** *131* (16), 5851-5857.
(20) Xie, Y.; Meng, Y. Sers Performance of Graphene Oxide Decorated Silver Nanoparticle/Titania Nanotube Array. *RSC Adv.* **2014,** *4*, 41734-41743.
(21) Wang, C.; Meng, D. L.; Sun, J. H.; Memon, J.; Huang, Y.; Geng, J. X. Graphene Wrapped Tio2 Based Catalysts with Enhanced Photocatalytic Activity. *Adv. Mater. Interfaces* **2014,** *1* (4), 1300150.
(22) Voinova, M. V.; Rodahl, M.; Jonson, M.; Kasemo, B. Viscoelastic Acoustic Response of Layered Polymer Films at Fluid-Solid Interfaces: Continuum Mechanics Approach. *Phys. Scr.* **1999,** *59*, 391–396.
(23) Panfilova, E. V.; Khlebtsov, B. N.; Burov, A. M.; Khlebtsov, N. G. Study of Polyol Synthesis Reaction Parmeters Controlling High Yield of Silver Nanocubes *Colloid J.* **2012.,** *74*, 99-109.
(24) Rycenga, M.; Xia, X.; Moran, C. H.; Zhou, F.; Qin, D.; Li, Z.-Y.; Xia, Y. Generation of Hot Spots with Silver Nanocubes for Single-Molecule Detection by Surface-Enhanced Raman Scattering. *Angew. Chem Int. Ed.* **2011,** *50*, 5473-5477.
(25) Ahamad, N.; Ianoul, A. Using Phospholipids to Control Interparticle Distance in Sers-Active Substrates *J. Phys. Chem. C* **2011,** *115*, 3587-3594.
(26) Mahmoud, M. A.; Tabor, C. E.; El-Sayed, M. A. Surface-Enhanced Raman Scattering Enhancement by Aggregated Silver Nanocube Monolayers Assembled by the Langmuir-Blodgett Technique at Different Surface Pressure. *J. Phys. Chem. C* **2009,** *113*, 5493-5501.
(27) Mahmoud, M. A.; El-Sayed, M. A. Comparative Study of the Assemblies and the Resulting Plasmon Fields of Langmuir-Blodgett Assembled Monolayers of Silver Nanocubes and Gold Nanocages. *J. Phys. Chem. C* **2008,** *112*, 14618-14625.
(28) Gambinossi, F.; Banchelli, M.; Durand, A.; Berti, D.; Brown, T.; Caminati, G.; Baglioni, P. Modulation of Density and Orientation of Amphiphilic DNA Anchored to Phospholipid
Membranes. I. Supported Lipid Bilayers. *J. Phys. Chem. B* **2010,** *114*, 7338-7347.

(29) Shen, X.; Lin, X. Y.; Yousefi, N.; Jia, J. J.; Kim, J. K. Wrinkling in Graphene Sheets and Graphene Oxide Papers. *Carbon* **2014,** *66*, 84-92.
(30) Zheng, Q. B.; Ip, W. H.; Lin, X. Y.; Yousefi, N.; Yeung, K. K.; Li, Z. G.; Kim, J. K. Transparent Conductive Films Consisting of Ultra Large Graphene Sheets Produced by Langmuir-Blodgett Assembly. *ACS Nano* **2011,** *5* (7), 6039-6051.
(31) Cote, L. J.; Kim, F.; Huang, J. Langmuir Blodgett Assembly of Graphite Oxide Single Layers. *J. Am. Chem. Soc.* **2009,** *131*, 1043-1049.
(32) Bi, H. C.; Yin, K. B.; Xie, X.; Ji, J.; Wan, S.; Sun, L. T.; Terrones, M.; Dresselhaus, M. S. Ultrahigh Humidity Sensitivity of Graphene Oxide. *Sci. Rep.* **2013,** *3*, 2714.
(33) Hao, L.; Mattevi, C.; Gallop, J.; Goniszewski, S.; Xiao, Y.; Cohen, L.; Klein, N. Microwave Surface Impedance Measurements on Reduced Graphene Oxide. *Nanotechnology* **2012,** *23* (28), 285706.
(34) Guo, F.; Kim, F.; Han, T. H.; Shenoy, V. B.; Huang, J.; Hurt, R. H. Hydration-Responsive Folding and Unfolding in Graphene Oxide Liquid Crystal Phases. *ACS Nano* **2011,** *5*, 8019-8025.
(35) Matteini, P.; Tatini, F.; Cavigli, L.; Ottaviano, S.; Ghini, G.; Pini, R. Graphene as a Photothermal Switch for Controlled Drug Release. *Nanoscale* **2014,** *6*, 7947-7953.
(36) Lu, G.; Mao, S.; Park, S.; Ruoff, R. S.; Chen, J. Facile, Noncovalent Decoration of Graphene Oxide Sheets with Nanocrystals. *Nano Res.* **2009,** *2*, 192-200.
(37) Zheng, Q.; Shi, L.; Ma, P. C.; Xue, Q.; Li, J.; Tang, Z.; Yang, J. Structure Control of Ultra-Large Graphene Oxide Sheets by the Langmuir-Blodgett Method *RSC Adv.* **2013,** *3*, 4680-4691.
(38) Wang, F.; Liu, J. W. Evaporation Induced Wrinkling of Graphene Oxide at the Nanoparticle Interface. *Nanoscale* **2015,** *7* (3), 919-923.
(39) Huh, S.; Park, J.; Kim, Y. S.; Kim, K. S.; Hong, B. H.; Nam, J.-M. Uv/Ozone-Oxidized Large-Scale Graphene Platform with Large Chemical Enhancement in Surface- Enhanced Raman Scattering. *ACS Nano* **2011,** *5*, 9799–9806.